SUPPLEMENT TO THE *WELDING JOURNAL*, JUNE 2009
Sponsored by the American Welding Society and the Welding Research Council

Vision-Based Spatter Classification for Contaminant Detection

Optical monitoring with a high-speed camera is used to evaluate the relationship between spatter and contaminants, such as oil and paint

BY G. SCHWAB, J. P. H. STEELE, AND T. L. VINCENT

ABSTRACT

This paper presents a new method for measuring and classifying spatter in gas metal arc welding (GMAW) by optical monitoring of the weld pool and surrounding area via a high-frame-rate camera. Image processing and tracking algorithms are described that extract and classify individual spatter events from raw camera images. This new sensor is then used to investigate the relationship between workpiece contamination and weld spatter.

Introduction

Spatter can be defined as the ejection of molten material from the weld pool during the welding process. Generally spatter is a signal that the process parameters (including materials, wire, and gasses) may not be optimal. Spatter mechanisms have been studied by a number of researchers (Refs. 1–7). Most of the attention has been on short circuit gas metal arc welding (GMAW) (Refs. 1–3) because of the level of spatter typically involved. Spatter has also been investigated for shielded metal arc welding (SMAW) and flux cored arc welding (FCAW)(Refs. 4, 6). In the case of FCAW, as in the case of short-circuit GMAW, arc stability was shown to be an important factor in the generation of spatter. Spatter is an important factor in most welding processes because of the cost of subsequent removal of the spatter and the potential for the spatter to cause in-service defects (Ref. 6), i.e., spatter can become nucleation sites for pit corrosion and microcracks. However, spatter can have other causes and be an indicator of poor weld quality. It is our hypothesis that spatter can signal the existence of weld contamination, and moreover, that the observed properties of the observed spatter can be useful for contaminant identification. Thus while previous work on the identification, quantification, and classification of spatter has been focused on the mechanisms within the welding process that cause spatter, this work is focused on the identification and classification of weld spatter as an indicator of the presence of containments. As welders know, if the arc comes in contact with external contaminants, it is often the case that the amount and type of spatter will change. Developing a method for identifying and quantifying those changes is the long-term goal of this project.

This paper discusses an image-based method for monitoring spatter in a GMAW process. In the work presented here, a CCD camera is used to monitor the weld pool and surrounding area. Spatter is identified and tracked so that the number of individual spatter events can be determined. Qualities of the spatter, such as size, direction, and velocity, are extracted. Here the spatter monitoring method is applied in a series of experiments using bead-on-plate gas metal arc welding of A36 steel. Oil and paint are intentionally introduced as contaminants, and the differences in the quantity and behavior of the generated spatter are observed.

KEYWORDS

CCD Camera
Gas Metal Arc
Optical Monitoring
Sensors
Spatter
Weld Pool

G. SCHWAB (gunther.schwab@gmail.com), J. P. H. STEELE (jsteele@mines.edu), and T. L. VINCENT (tvincent@mines.edu) are with the Engineering Division, Colorado School of Mines, Golden, Colo.

Other work has utilized cameras as a sensor for robotic welding (Refs. 8–12), but primarily for the purpose of measuring weld geometry or joint tracking. None has considered spatter monitoring. One of the intended outcomes of this research is to develop a new method for fault detection in GMAW that can be applied in real-time to reduce rework, and improve quality and productivity.

Vision-Based Spatter Classification

Experimental Hardware and Example Data

The laboratory setup for the experiments consists of a FANUC ARC Mate 100i robot, a Lincoln Electric Power Wave 455 power source, and a Tregaskiss welding gun. In order to obtain images of the weld pool and surrounding area, a Basler A504k high-speed camera was mounted to the robot arm, as shown in Fig. 1. The camera was attached at a point such that the backplane of the camera was 0.3 m from the tip of the welding gun and positioned to view an area of about 150 × 115 mm around the weld pool. An acrylic encasement protects the camera from spatter. The camera acquires images at up to 400 frames per second with an exposure time of 45 μs. Only very bright objects are visible at such short exposure times. A wide-angle lens (28 mm) was used to image the weld pool and plate, providing the ability to track spatter for a longer period of time. Because we are interested in imaging a large area around the weld arc, interference from the arc does not play a large role, and image acquisition does not need to be synchronized to the weld process. The images from the camera are transferred to the computer using two PCIe-1429 frame grabber boards manufactured by National Instruments. The image recording and processing takes place on a dual Xeon machine, using the

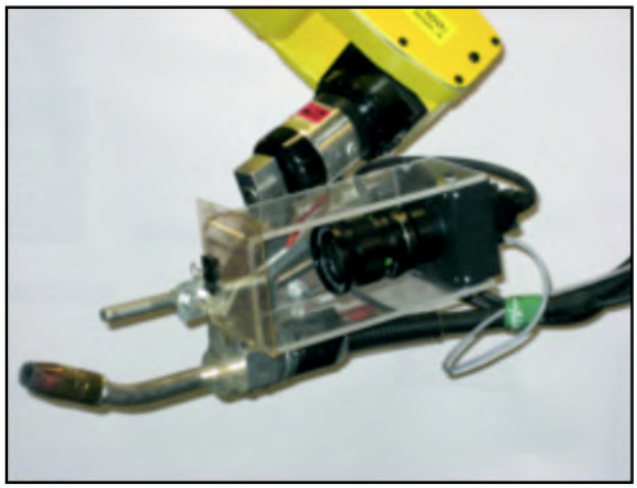

Fig. 1 — Spatter detection camera. A Balser A504k high-speed camera is mounted on the arm of the robot, about 300 mm from the welding gun tip.

National Instruments Vision Assistant 7.1 combined with Labview 8.20. The captured sequence of images is then post-processed to extract spatter events. An industrial version of this sensor could utilize efficient image processing implemented in hardware or field programmable gate array (FPGA) to enable real-time data processing, but this was not implemented in our prototype system.

An example of the raw data captured by the camera is shown in Fig. 2. The images are shown in inverted intensity so bright objects will show up as dark spots in these images. This is done here so that the spatter can be more easily picked out by the human eye; it is not part of the image processing for spatter tracking. Spatter in this figure appears as small, round, black objects; however, the images also contain the arc light and reflections of the arc light from the weld pool and welding fumes. In this figure three consecutive images are shown, taken at intervals of 2.5 ms. Note that the small dark spots that represent spatter move outward from the large annulus that is located at the welding arc to the edge of the image. By comparing the size of the spatter objects between images, and using our expectations for spatter behavior, one can mentally link together an object from each image that we expect corresponds to the same physical object, and thus isolate a single spatter event. The objective of this paper is to describe an automated method for processing the images to achieve the same result.

In order to be more precise in our language with discussing the various manifestations of spatter, the following terminology is used. The ejection of material from the weld pool and its subsequent flight is called a spatter event. Note for this work we assume that only one object is ejected per event. A feature (i.e., blob) in the camera image is called an object. That is, a spatter event is the physical manifestation of spatter in the real world, while a spatter object is what is recorded on the camera when the spatter event occurs. We further refine our nomenclature concerning spatter objects to distinguish between different points in the track estimation process. Those objects that pass through initial filtering via image processing are called potential spatter objects (or potential objects). The potential spatter objects that are selected to be part of a track by a tracking algorithm are detected spatter objects (or detected objects). A collection of detected spatter objects created by the same spatter event is a spatter track.

The goal of the data processing is to determine the number and character of the spatter events, where the spatter characteristics of interest include the amount of material ejected (size), the velocity, and the direction of flight. Since a single spatter event may cause a varying number of spatter objects depending on the velocity and temperature/brightness of the spatter, counting spatter events provides a more accurate characterization of spatter activity than simply counting the raw number of objects in each image. In addition, while image processing may remove the majority of spurious, nonspatter related objects, some may still be passed on as possible spatter objects. By linking objects into tracks, spurious objects are more easily identified.

In the next section, we discuss our proposed method for spatter monitoring in detail. First, some simple image processing is done to determine the location and size of potential spatter objects in the image. This information is then collected over a sequence of images and processed by a spatter tracker to determine which group objects correspond to one spatter event.

Image Processing and Spatter Tracking

The raw data collected by the camera is a 1280 × 1024 matrix of 8-bit unsigned integers, with small values corresponding to dark areas and large values corresponding to bright areas. The objective of the image processing step is to identify the locations in the image that correspond to small, round, bright objects. Image processing begins by quantizing pixels values to either one (bright) or zero (dark), via a preselected threshold, which is based on the overall intensity of the image, and is used to separate all pixels as either black or white. Because the welding arc and weld pool are always in the same location in the image, due to the camera's position being fixed relative to the welding gun, all pixels within the arc and weld pool are set to zero. Reflections of the arc off of welding vapors can cause a region of the image to contain a large number of isolated bright pixels. Since the objective of the image processing is simply to find potential spatter objects, rather than filter out noise, the quantized image is morphologically processed by a dilation operator to connect speckled areas into contiguous bright regions (Ref. 13). The structuring element for the dilation operator was a circle with a radius of 3 pixels, and thus the smallest object in the processed image will have a 3-pixel radius. This groups artifacts such as vapors into a single object without greatly affecting the true spatter image objects. The image artifacts will be removed either by shape classification, or by the tracking algorithm discussed later.

Since spatter objects should appear as approximately circular objects in the camera image, a measure of roundness is introduced by calculating the area and circumference of each object. The radius is then calculated from each using the formulas for the area and circumference of a circle. When the two radii are similar, the object is considered a potential spatter object and retained for further classification; otherwise it is disregarded from further processing.

The potential spatter objects are then classified according to size. Objects with an area of less than 35 pixels are considered small (0.7 mm diameter), those between 36 and 80 medium (0.7 to 1.3 mm), and those above large (greater than 1.3 mm). The sizes in mm correspond to a distance from the camera of about 300 mm.

After image processing, the image location, size, and associated image number for potential spatter objects are passed to a tracking algorithm. The purpose of the tracking algorithm is to aggregate raw spatter objects together into a track representing a single spatter event, as well as determining the velocity and direction of the spatter. Given an initial spatter object, a reasonable algorithm would be to connect this object to the closest object in the next frame that is farther away from the weld pool. However, there can sometimes be multiple reasonable choices. An example of the challenges in determining spatter tracks is shown in Fig. 3. Both the left and right images show the potential spatter objects for the same 30-image sequence, annotated by the image number that the object appears in. The tracks for

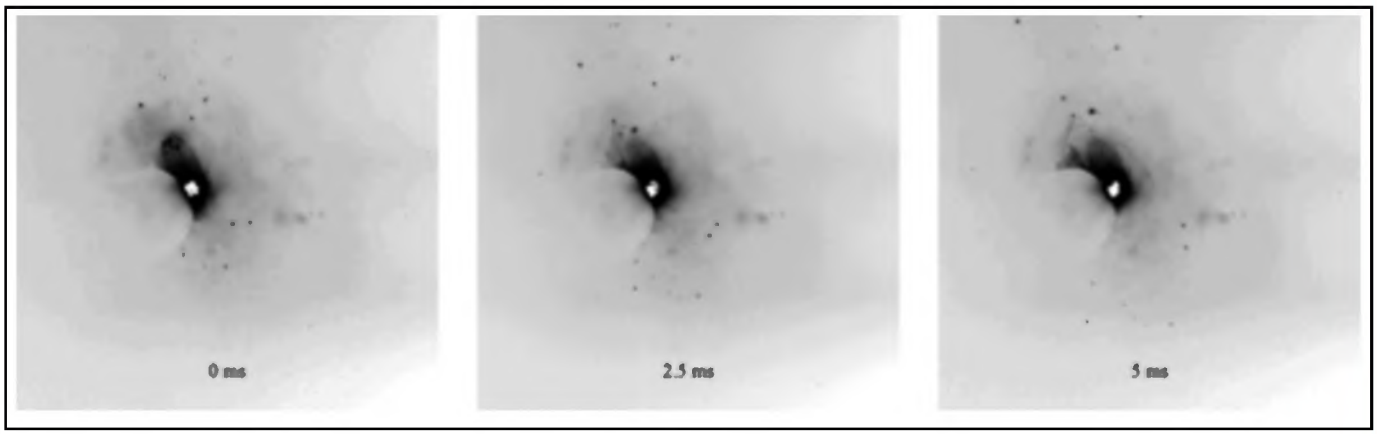

Fig. 2 — Inverse intensity image sequence during spatter event. Black points correspond to bright features. The large dark spot in the center is the weld arc. The white spot in the middle of the arc is an image artifact. The sequence progresses at 400 Hz from left to right.

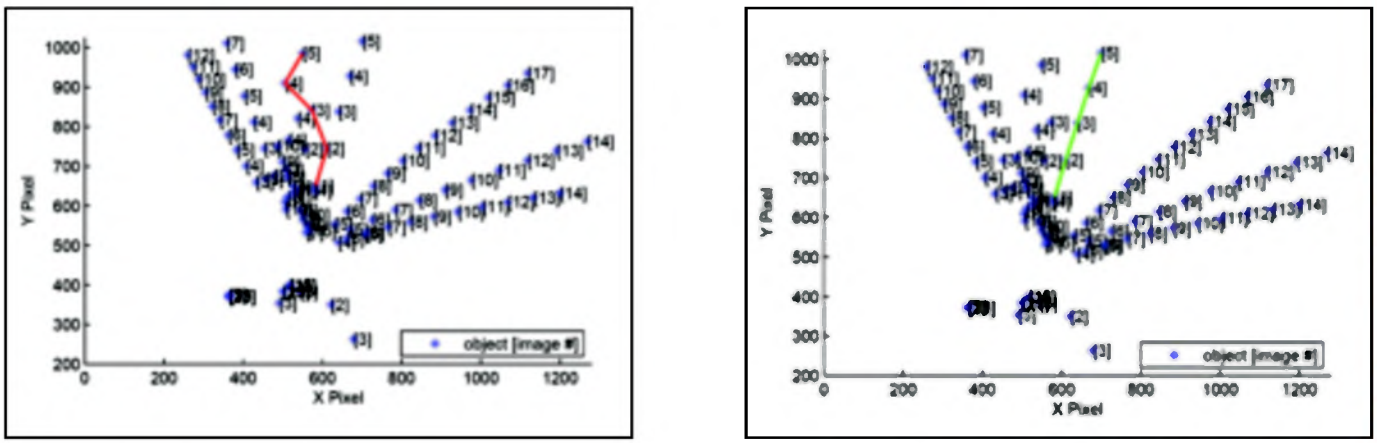

Fig. 3 — Illustration of track selection. The left and right images show potential spatter objects over a sequence of 30 frames, annotated by the image number that they appear in. The red line for the left image and green line on the right image connect potential spatter objects that occur in sequential frames. Although both tracks may be possible, the trajectory in green is much more likely.

many different spatter events can be visually detected, which can be generally segregated by time and distance. Two different choices for linking potential spatter objects into tracks are illustrated by the red line in the left image and green line in the right image. Note that both the red line and the green line connect objects that are close both in time and space. Thus, even if objects are only linked to other objects in neighboring frames that are within a fixed distance, there may be several different choices available for linking. This is especially true for slower frame rates, which allow spatter to have a greater distance of travel between frames. However, it is fairly easy (for a human) to judge that the green trajectory is much more likely to correspond to an actual spatter track than the red trajectory.

Further complicating the problem is that each potential track cannot be considered in isolation. Given the 2-D location and size of potential spatter objects over a series of image frames, a decision needs to be made regarding the disposition of each object. There are several possibilities. If the potential spatter object is thought to be caused by a spatter event, it can be linked to another object that is nearby in a neighboring frame. On the other hand, if the potential spatter object is though to be a false detection, it can be left out of a track. Once a decision has been made for each object, a complete decomposition of the potential spatter objects has been obtained. However, for the types of images created by spatter, many different decompositions may be possible. Choosing which objects belong with which track is at the heart of the problem of multiple target tracking, which is of great importance in applications such as tracking unknown aircraft using radar. Our approach uses a standard probabilistic method (Refs. 14–16), where the decision to create a track is based on the observed congruence with models of the spatter behavior and imaging process. That is, given our models, we calculate the probability that a particular decomposition is correct. The spatter and imaging models are described in more detail below. The estimated "best" decomposition is chosen as the one that maximizes this probability, i.e., the Maximum *A Posteriori* (MAP) criterion. The details of the algorithm are covered in Ref. 17, but an overview is given here.

Because spatter is a transient event, our problem is amenable to a semibatch approach. The image data are split up into groups of M sequential frames, with each group considered separately; spatter events that span two different sections will be combined later. Each frame within a group is indexed by the integer k, which runs from 1 to M. Thus, the time at which an image is taken, relative to the start of the sequence, is $t = kT_S$ where T_S is the sample rate of the camera (T_S = 1/400s in our case). In each group, decompositions of the potential spatter objects in the images are considered. Potential objects are linked together into tracks, such that no

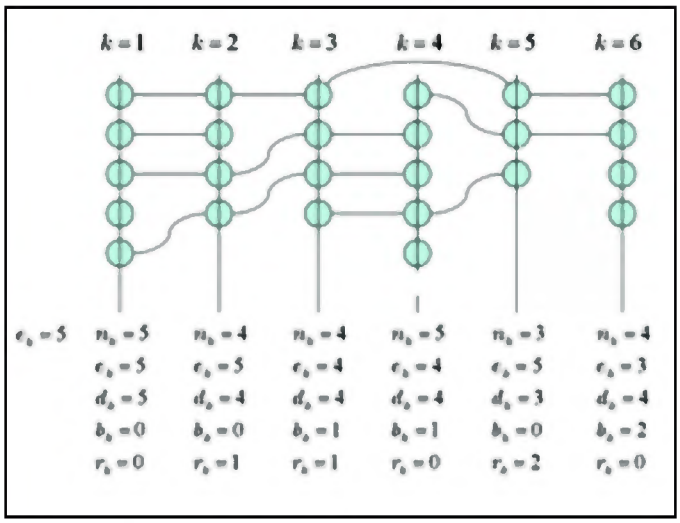

Fig. 4 — Example decomposition. Each vertical line represents a time at which an image was taken and each circle stands for a potential object. The links indicate a track, and a set of tracks is a decomposition.

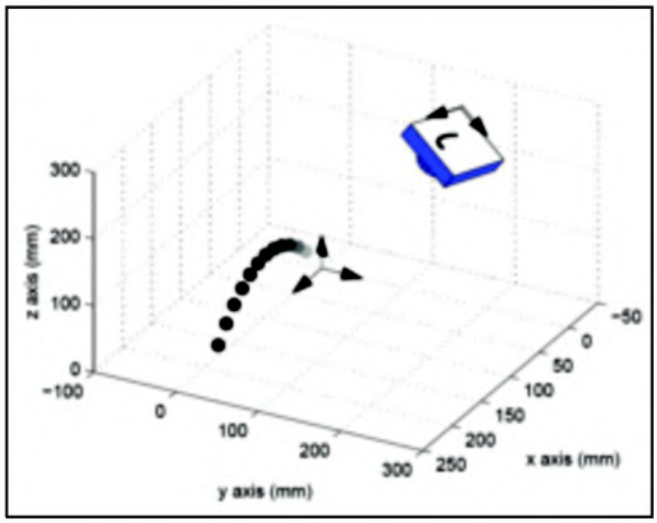

Fig. 5 — Illustration of spatter path and imaging process. The world coordinate system is centered at the weld pool. The camera observes this process at a fixed position and orientation relative to the world coordinates.

object is contained in two tracks. Figure 4 shows an example of such a decomposition. Each vertical line represents a separate image frame and each circle stands for a potential object. The objects are linked by horizontal lines to indicate a track, and a set of tracks is a decomposition. Thus, horizontal lines that connect objects into a track are analogous to the lines drawn in Fig. 3, but in Fig. 4, the position of the objects in the image is no longer shown, just which object corresponds to a particular frame. Note that a track may skip an image, denoting a missed detection, and that some objects are not linked, denoting a false detection. The variables below each line characterize the track decomposition and are used to determine the likelihood of that decomposition. The calculation of this likelihood is described next, and the discussion of these variables follows.

Let Z be the set of data for the section (the location and frame number of all potential objects), and let D denote a decomposition of that data into tracks and false detections (a particular choice for horizontal lines in Fig. 4). The probability that D is correct given the data Z (that is, the *a posteriori* probability) is denoted $P(D|Z)$. By Bayes's Rule (Ref. 18), this probability can be calculated as

$$P(D|Z) = \frac{1}{c} P(Z|D) P(D) \quad (1)$$

where $P(Z|D)$ is the probability of the observed data given the decomposition is correct, and $P(D)$ is the *a priori* probability of decomposition D occurring. The constant c scales the probability distribution so that it integrates to one; however, when maximizing the probability function, this scale factor is irrelevant.

This can be interpreted as follows: There are two aspects by which a particular decomposition is judged — the likelihood of the individual tracks within a decomposition, and the likelihood of the detections implied by the decompositions, such as the number of missed detections, false detections, and track starts and stops. Both of these are necessary, as there is a tradeoff between how closely tracks will fit the spatter behavior and the chosen number of tracks and false detections. For example, consider a group of frames that observes a single spatter event, resulting in a single arc of potential spatter objects. Will our algorithm link these objects together into a track? Because there are always uncertainties, disturbances, or noise that cannot be modeled deterministically, one would get the best fit to the spatter behavior model by linking just two spatter objects, and calling all other objects false detections. Linking all the objects together will result in a track that has a slightly less good fit to the model, and thus a slightly lower conditional probability $P(Z|D)$. However, if the corresponding reduction in the number of false detections results in a much higher probability of the decomposition $P(D)$, and thus an increase in $P(D|Z)$, our algorithm will decide to (correctly) link all other objects together into a track. Thus, our objective will be to maximize the product of the track and decomposition probabilities. Note that in practice, the natural log of the probability functions is utilized in order to improve numerical stability (Ref. 16).

In order to describe in more detail the calculation of $P(Z|D)$ and $P(D)$, the following are defined. Suppose there are N tracks. For track i connecting ℓ_i objects across several frames, we define the matrix

$$Y_i = \left[y_1 \; y_2 \cdots y_{\ell_i} \right]^T \quad (2)$$

where $y_j = [u_j \; v_j]^T$ is the pixel location in the image of the jth object in the track. For image number k in the group, additional variables are defined that characterize the likelihood of the types of objects in this image, specifically

$$D_k = \left[n_k \; e_k \; d_k \; b_k \; r_k \right]^T \quad (3)$$

where the definitions for these variables are given in Table 1. Note that the values of these variables are listed in the bottom of Fig. 4 for that particular example.

Table 1 — Definition of Variables that Characterize a Decomposition

n_k	Number of observations for image k
e_k	Number of tracks for image $k-1$
d_k	Number of detections for image k (number of circles for image k with lines to either the left or right)
b_k	Number of new tracks for image k (number of circles for image k)
z_k	Number of tracks terminated for image k (number of circles for image $k-1$ with a line only to the left)

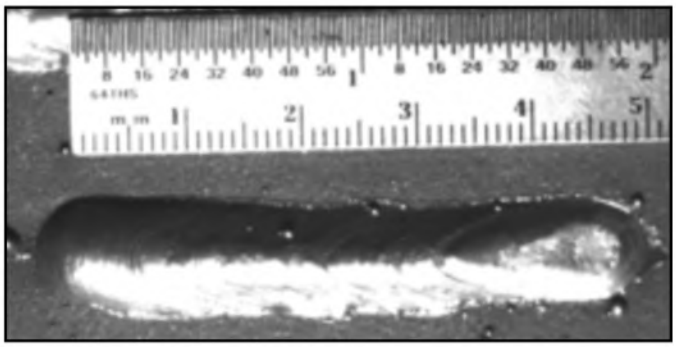

Fig. 6 — Constant voltage reference weld.

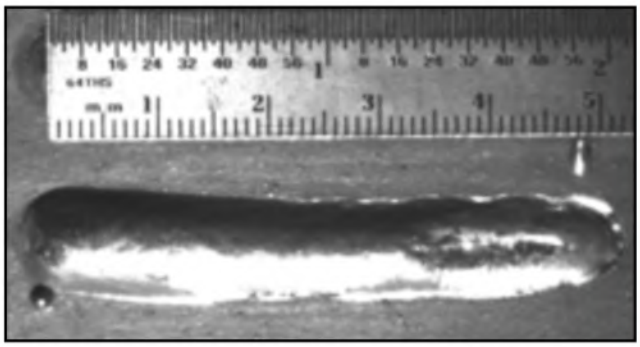

Fig. 7 — Pulsed reference weld.

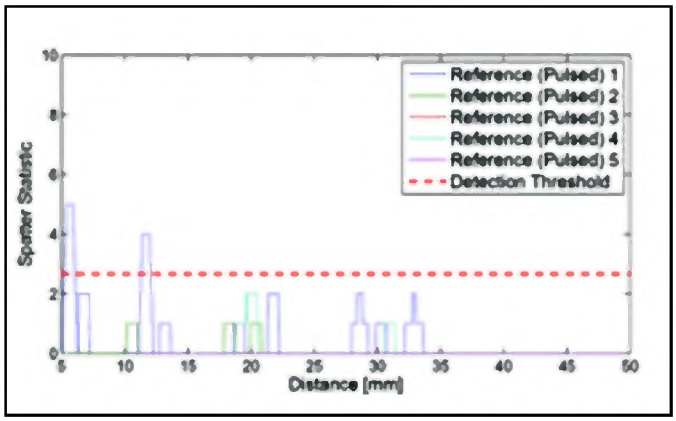

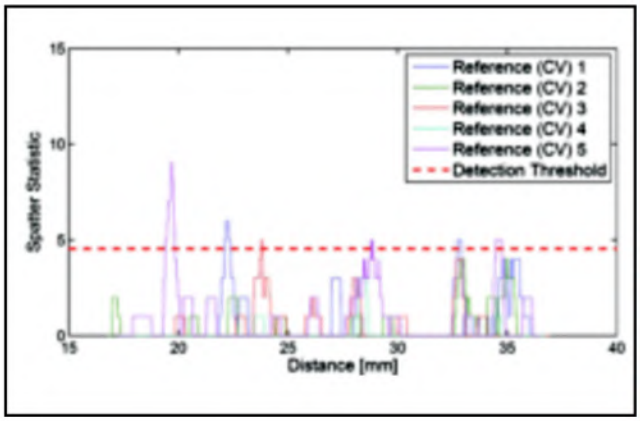

Fig. 8 — Nominal spatter behavior. Plot of the spatter statistic vs. torch position relative to the start of the weld. A — Constant voltage process; B — pulsed process.

a priori Decomposition Probability

The form of the *a priori* decomposition probability density $P(D)$ depends on the characteristics of the spatter events (e.g., how many and how they are distributed in time) and the imaging/image processing system (e.g., number of false and missed detections, and their distribution in time) .A complete characterization of $P(D)$ for any one system could be time consuming to obtain, but for the purposes of spatter tracking, only an approximate model is necessary.

For our implementation, it is assumed that the number of new spatter events over each time interval T_s follows a Poisson distribution with mean λ_b. Defining b_k to be the number of spatter events initiated during image k, the probability density for b_k is given by

$$p_b(b_k) = e^{-\lambda_b}\left(\frac{\lambda_b^{b_k}}{b_k!}\right) \quad (4)$$

Similarly, the number of false detections for image $f_k = n_k - d_k$ for image k are assumed to follow a Poisson distribution with mean λ_f.

Furthermore, we assume that the probability of an existing track terminating at image k is p_z, and the probability of the track being detected at image k is p_d. The probability of observing r_k terminations and d_k detections is then, respectively

$$p_z(r_k) = \binom{e_k}{r_k} p_z^{r_k}(1-p_z)^{e_k - r_k}$$

$$p_d(d_k) = \binom{e_{k+1}}{d_k} p_d^{d_k}(1-p_d)^{e_{k+1}-d_k}$$

If the spatter events, track terminations, false detections, and missed detections are independent, then the probability of observing the decomposition D_k for the image at time t is

$$p(D_k) = p_b(b_k)\,p_f(n_k - d_k)\times p_z(r_k)\,p_d(d_k) \quad (5)$$

Under the additional assumption that the events at different times are independent, the probability distribution for the complete decomposition D is given by

$$p(D_k) = \prod_{t=1}^{M} p(D_k) \quad (6)$$

Track Probability

The conditional probability $P(Z \mid D)$ is based on a ballistic model for the spatter droplet, and a pinhole camera model. Let

$$x = \begin{bmatrix} x_x & x_y & x_z \end{bmatrix}^T \quad (7)$$

be the location of the spatter in a coordinate system with origin in the center of the weld pool and the z axis pointing upward. (Since the weld pool moves much more slowly than the spatter, this can be considered a fixed coordinate system.) Assuming viscous damping, gravity, and a random disturbance force w, the free flight motion of spatter can be described by

$$\ddot{x} + \gamma\dot{x} = -g + w \quad (8)$$

γ represents the damping coefficient, $g = [0\ 0\ 9.81]'$ is gravitational acceleration. The parameters are normalized by the mass of the droplet. Since the spatter is

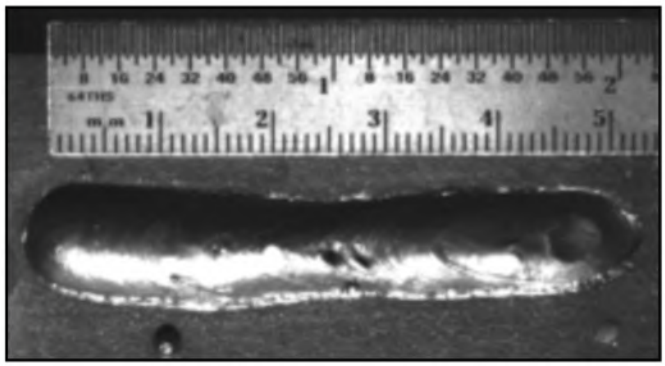

Fig. 9 — Weld bead after constant voltage weld over 0.15-mm paint contamination.

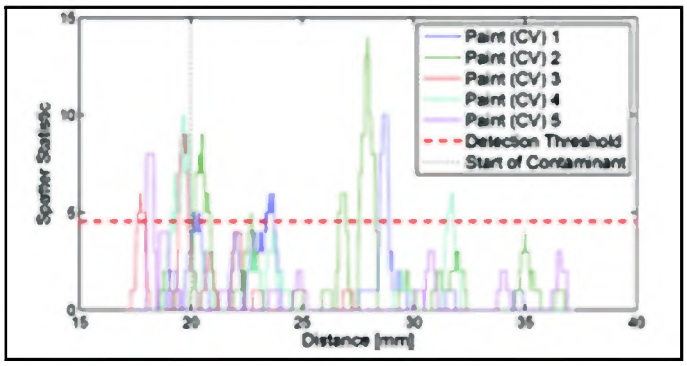

Fig. 10 — Plot of the spatter statistic vs. welding gun position relative to the start of the weld for 0.15-mm paint contamination, constant voltage weld. The start of the contaminant is indicated by the vertical dotted line.

observed only at discrete moments in time, we utilize a discrete time model that is equivalent at the sample times $t = kT_S$. With a state vector z_k containing the position and velocity at time kT_S, that is,

$$z_k = \left[x(kT)^T \quad \dot{x}(kT)^T \right] \tag{9}$$

and assuming that w is constant over the sampling time interval, the equivalent discrete time model can then be written as

$$z_{k+1} = \begin{bmatrix} I\frac{1}{\gamma}\left(1-e^{-\gamma T_s}\right)I \\ 0 \quad e^{-\gamma T_s} I \end{bmatrix} z_k - \begin{bmatrix} \frac{1}{\gamma}T_s - \frac{1}{\gamma^2}\left(1-e^{\gamma T_s}\right)I \\ \frac{1}{\gamma}\left(1-e^{-\gamma T_s}\right)I \end{bmatrix} g + w_k \tag{10}$$

where $w_k = w(kT_S)$ and I is the 3×3 identity matrix. It is assumed that w_k is a zero mean, Gaussian white noise random sequence with covariance QT_S. To simplify notation, Equation 10 will be written as

$$z_{k+1} = g(z_k) + v_k \tag{11}$$

An example of a spatter path is shown in Fig. 5, with the camera represented by the blue rectangular solid. The image of the spatter path is placed on the back of the camera.

This three-dimensional path is then transformed into a two-dimensional image using an ideal camera projection model. The camera projection model converts the calculated 3-D points into the 2-D pixel locations of the image plane. As shown in Fig. 5, the camera lies at a fixed position and orientation relative to the world coordinate system located at the weld pool. A camera coordinate system is attached to the camera, with x and y axes parallel to the image plane, and the z axis pointing outward along the center axis of the camera lens. The rotation R and translation t that maps the representation of points in the world coordinate system to the camera coordinate system can be obtained using a camera calibration method (Ref. 19). Once in the camera coordinate system, points are then projected into the image plane using the camera's focal length f, image size and image center c_0. As only integer numbers of pixels are possible, the results of this transformation are rounded to the nearest integer. The observation model for spatter is given by

$$y_k = p(Rx_k + t) + c_0 + n_k \tag{12}$$

where p is the perspective projection,

$$p(x) = \begin{bmatrix} f\frac{x_x}{x_z} \\ f\frac{x_y}{x_z} \end{bmatrix} \tag{13}$$

and n_k is the observation noise. It is assumed that n_k is a zero mean, Gaussian white noise random sequence with covariance C. For simplicity, the observation model (Equation 12) will be notated as

$$y_k = h(z_k) + n_k \tag{14}$$

Finally, the initial state is assumed to follow

$$z_1 = e_1 \tag{15}$$

where e_1 is a zero mean, Gaussian random variable with covariance P_1.

With the spatter model defined by Equations 11, 14, and 15, the conditional probability of observing object track given that the track decomposition is correct can be approximately computed using a (smoothing) Extended Kalman Filter (Ref. 20), which finds $z_1, z_2, \ldots, z_{\ell_i}$ to minimize

$$L(z_1, z_2, \ldots z\ell_i) = (z_1 - \hat{z}_1)^T P_1^{-1}(z_1 - \hat{z}_1) + \sum_{k=1}^{\ell_i} (y_k - h(z_k))^T C^{-1}(y_k - h(z_k)) + \sum_{k=1}^{\ell_i - 1} (z_{k+1} - g(z_k))^T (QT_s)^{-1}(z_{k+1} - g(z_k)) \tag{16}$$

subject to the constraints defined by Equa-

Table 2 — Algorithm Parameters

M	Q	C	P_1	λ_b	λ_f	p_z	p_d
30	20	1	10^5	0.1	0.01	0.16	0.9

Table 3 — Baseline Parameters

Process	Voltage/Trim	WFS	Travel Speed	Standoff	Frame Rate/s
CV	28 V	325 in./s	6 mm/s	17 mm	400
Pulsed	1.2	275 in./s	6 mm/s	12 mm	200

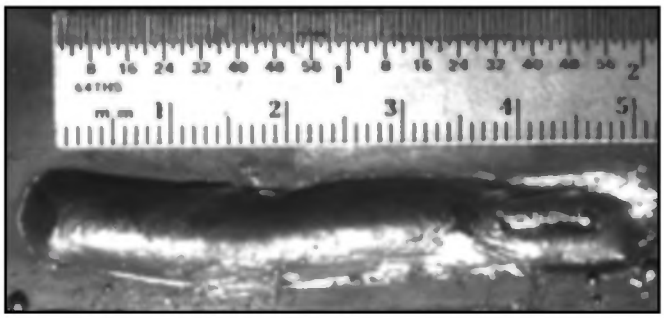

Fig. 11 — Weld bead after pulsed weld over 0.15-mm paint contamination.

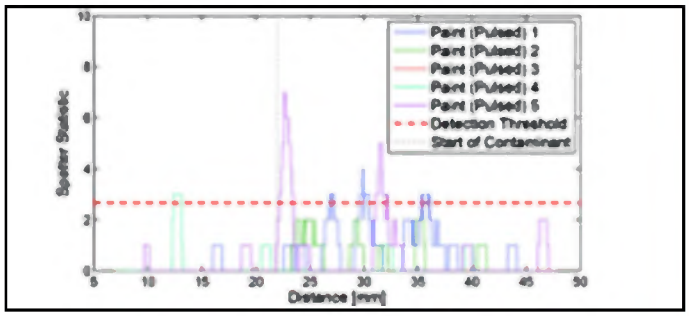

Fig. 12 — Plot of the spatter statistic vs. welding gun position relative to the start of the weld for 0.15-mm paint contamination, pulsed weld. The start of the contaminant is indicated by the vertical dotted line.

tions 11 and 14 (with appropriate modifications for missed detections). Let $\hat{z}_t^i, P_t^i$ be the resulting estimate and (approximate) error covariance, and set

$b_t^i = C\hat{z}_t^i, B_t^i = CP_t^iC' + R.$ The track probability is then given by

$$p(Y_i) = \prod_{k=1}^{N_i} N\left(y_{t_k}^i \middle| b_{t_k}^i, B_{t_k}^i\right) \quad (17)$$

where $N(x|\mu,\Sigma)$ denotes a Gaussian distribution with mean μ and covariance Σ. The probability of the observed data given decomposition D is then the product of the probabilities for the individual tracks.

$$p(Z|D) = \prod_{i=1}^{N} p(Y_i) \quad (18)$$

Data Processing

Given the decomposition metric defined by Equation 1, data processing for each group of frames consists of linking potential spatter objects into tracks, and searching for the decomposition with the highest probability. The choices of parameters for our implementation are given in Table 2. Since the number of possible tracks scales factorially with the number of objects, practical application requires avoiding linking objects that have an obvious low probability of being in the same track, a process that is called gating. For the spatter tracking applications, the gating constraints placed on object linking are the following:

- Only link to objects in the next or subsequent frame (allow only one missed detection in a row).
- Only link to objects located less than d pixels away in the next frame, or $2d$ pixels away in the subsequent frame.
- Only link to objects of the same size class (small, medium, or large).

Other gating constraints are possible, such as limiting links to an arc centered at the weld pool, but were not included in our off-line implementation. With proper gating, the computational expense of the maximum-likelihood tracking algorithm can be quite modest compared to the raw image processing needed to extract potential spatter objects. Indeed, in most frames, there will be few objects that need to be considered. It is possible that simply counting raw potential spatter objects could be used for diagnosis, but since the number of spatter events is more directly connected with the physical process, it is an advantage to pursuing the spatter events approach. In addition, just using the raw count would not provide any information about the velocity of the spatter objects. In the work presented here, the velocity of large spatter objects varied with the type of contaminant. Thus velocity could potentially be important to the diagnosis.

The search proceeds in three stages. First, in the initialization stage, objects are chosen as potential track seeds. In order to reduce the number of other object satisfying the gate constraints, seed objects are chosen outside of a circle centered at the weld pool, where the distance between tracks is larger. Tracks are then iteratively extended off of these seed objects and continuing along objects satisfying the gating constraints of the last object in the track. New objects are accepted if they are not part of another track, and the net a-posteriori decomposition probability increases when they are part of a track.

Once track initialization has been attempted from all seed objects, a refinement stage occurs. There are five operations that occur on tracks in the refinement stage. The result of these operations is accepted if it results in an increase in the *a posteriori* decomposition probability.

- Extend forward: An object that does not belong to another track and satisfies the gating constraints of the last object in the track is linked.
- Extend back: An object that does not belong to another track and for which the first object in the track satisfies the gating constraints is linked.
- Split: A track is split into two tracks.
- Merge: The end of one track is linked to the beginning of another track that satisfies the gating constraints.
- Removal: The links to a track that is 3 objects or less are removed.

These operations are randomly applied to links until either no further improvement is achieved, as measured by a certain consecutive number of rejected operations, or a fixed number of attempts have been tried.

Finally, after each group was processed, tracks that ended at the last image in the group, or began at the first image of the group, were compared against neighboring groups to determine if they could be connected across group boundaries.

Experimental Procedure

The objective of the development of the spatter tracking algorithm is to determine if spatter is a useful metric for the identification of contaminants in welding. To demonstrate its potential, a series of bead-on-plate experiments was performed on nominal and contaminated material, using both a constant voltage and pulsed welding process. In this section is described the weld process settings, baseline spatter rate, and process for creating contaminated weld plates.

Establishing the Nominal Weld Process

To create the nominal weld process, settings were found for both constant voltage and pulsed processes that yielded a good weld with a smooth, even surface with no cracks, no visible porosity or void spaces, no undercut along the edge, and a shallow toe angle. The frame rate of the camera was also varied between the two processes. The constant voltage (CV) process generated more spatter, and a

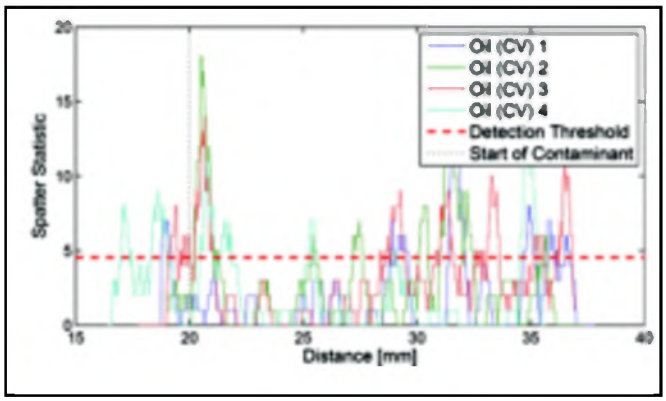

Fig. 13 — Plot of the spatter statistic vs. welding gun position relative to the start of the weld for heavy oil contamination, constant voltage weld. The start of the contaminant is indicated by the vertical dotted line.

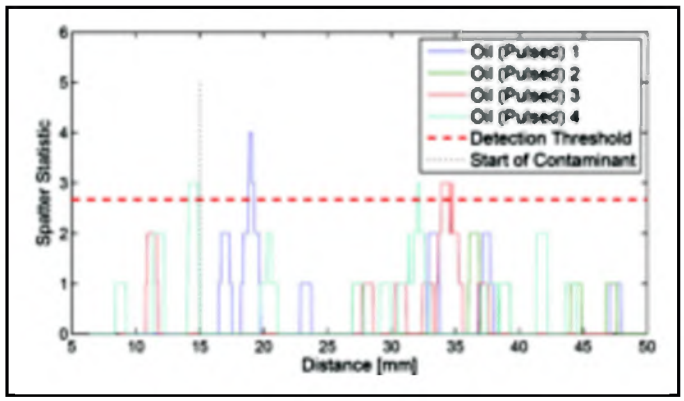

Fig. 14 — Plot of the spatter statistic vs. welding gun position relative to the start of the weld for heavy oil contamination, pulsed weld. The start of the contaminant is indicated by the vertical dotted line.

higher frame rate simplified the processing by limiting the travel distance of spatter objects. The optimal parameters found are displayed in Table 3. Note that different camera frame rates were chosen for the two different processes. A lower frame rate increases the length of weld covered by a fixed number of frames, but makes the spatter tracking more difficult, as spatter will move father between frames. Thus, a higher frame rate produces more data, but reduces the search space for establishing spatter tracks. Within this tradeoff a frame rate can be chosen to reduce the computational load. Constant voltage weld processing had a higher amount of spatter and required the higher frame rate to process the data.

Figures 6 and 7 show examples of welds created using a constant voltage process and a pulsed process, respectively. As the available gas mixture of 75% argon and 25% CO_2 was not ideally suited for the pulsed process, the appearance of those welds is not optimal.

A certain level of spatter is present even in the absence of contamination. This level varies with the type of process used. For example, in pulsed welding the amount of spatter created is generally significantly less than in constant voltage welding. In order to determine whether the observed increase in the spatter level was statistically significant, a baseline level had to be found. Based on preliminary analysis of the data, the number of spatter events larger than 1.3 mm had the largest variation between processes, and thus, it was postulated that this contained information relevant for fault detection. Thus, we chose the statistic to monitor as the number of spatter events larger than 1.3 mm in diameter that occur in a window of 30 frames centered around the current time. A window of 30 frames corresponds to a welding gun travel distance of about 0.5 mm along the weld at 400 ft/s frame rate (the travel speed was 6 mm/s).

Assuming that spatter events at each frame are independent of each other and follow a Poisson distribution with parameter λ, the distribution of the spatter statistic, at a fixed time will also be Poisson with expected value 30λ. Thus, the probability distribution for *s*, the number of spatter events in the window, is

$$p_s(s) = 30\lambda^s \frac{e^{-30\lambda}}{s!} \qquad (19)$$

Five welds were performed on uncontaminated plates for both constant voltage and pulsed welding processes. The parameter λ was determined by finding the average number of events per frame for all reference welds (of the same frame rate and for the same process). A nominal spatter level was set as the 99.9% level of the Poisson distribution. That is, the nominal spatter level was set such that the nominal process will have a spatter statistic below this level for 99.9% of the time. The nominal spatter detection levels were found to be 4.54 events for the continuous voltage process, and 2.67 events for the pulsed process. Plots of the spatter events for the nominal processes are shown in Fig. 8.

Table 4 — Experimental Results for the Constant Voltage Welding Processes

Cont.	Events	Avg. Vel.	Max. Vel.	Avg. Size
Oil: light	259.8	18.2	77.5	62.5
Oil: heavy	408.5	16.3	95.5	67.8
Paint: one layer	306.0	20.9	79.5	61.9
Paint: two layers	203.8	20.8	76.0	66.9
Paint: three layers	189.8	19.2	71.6	65.17
Reference	127.0	23.7	79.2	59.7

Table 5 — Experimental Results for the Pulsed Welding Process

Cont.	Events	Avg. Vel.	Max. Vel.	Avg. Size
Oil: light	33.3	38.1	140.4	82.1
Oil: heavy	44.8	37.4	82.7	76.7
Paint: one layer	19.2	45.3	82.2	76.2
Paint: two layers	24.4	30.8	83.9	82.7
Paint: three layers	30.8	27.7	72.1	94.3
Reference	19.3	42.2	112.8	75.7

Preparation of Contaminated Plates

In order to obtain realistic conditions, mild steel plates with a thickness of 9 mm for constant voltage welding and 3 mm for pulsed welding were prepared with the different contaminants.

Paint

For paint, the contaminant was applied in a one-in.-wide area perpendicular to the travel direction of the welding gun. The paint was applied with a foam brush. In order to obtain different thicknesses, one layer was applied, given time to dry and then another layer was applied over it. The resulting total thickness was measured using a dial indicator mounted on a linear positioner. One layer had a thickness of roughly 0.03 mm, two layers about 0.06 mm, and three layers about 0.15 mm.

Oil

As oil remains in liquid state and tends to spread out over the plate, it was not possible to guarantee an exact amount per area. To be as consistent as possible, a fixed number of drops of oil were applied to the plate and spread out over the desired area with a brush. The experiment was carried out immediately after this application.

Results and Discussion

Five welds were performed for each level of paint contaminant, and four welds were performed for each type of oil contaminant. During the weld, 1200 image frames were collected and analyzed for spatter events. The number of spatter events (that is, number of tracks) was tabulated, along with size of the object in the track in pixels, and the velocity of the track across the image in pixels per second as measured by the first two objects in the track. Statistics of the results are given in Tables 4 and 5. To eliminate the influence of stationary objects that prevail for several frames, tracks that have a pixel velocity of zero were removed. These objects could be reflections of the arc off of fumes or the part itself, and since their position in the image frame is variable, they cannot be removed by masking in the same way as was done with the arc itself. This filtering process is enabled by estimating the track velocity. Note also that the average velocity of the objects varies with contaminant type. Although the velocity was not included as part of our spatter statistic, this would be an interesting area for future investigation.

For the constant voltage process, an increase in spatter events is evident for all contaminated welds, with the largest increase for heavy oil contamination. Interestingly, while at least 1.5 times greater than the number of spatter events in the reference (no contamination case), the number of spatter events seems to decrease with increasing layers of paint. The average spatter size is fairly consistent, but does appear to increase slightly for higher levels of contamination.

The pulsed wave process also shows an increase in spatter events for all contaminated welds except for one layer of paint. Note that the number of spatter events is much smaller than for the constant voltage process. In this case, spatter events increase with increasing levels of contamination, along with a general trend of larger spatter objects.

In the next sections, the spatter behavior is examined in more detail for the highest levels of contamination.

Paint

Of the two contaminants examined in the constant voltage process, paint was the one that caused the most severe observed changes to the weld bead. However, the severity of the reaction depended heavily on the thickness of the paint. It is likely that thin layers of paint vaporized before interaction with the weld pool could occur. However, for the thickest application (0.15 mm) enough paint remained to react violently with the molten metal, causing explosions in the pool that led to the ejection of large amounts of material as well as gas bubbles that solidified, causing porosity. Figure 9 shows an example of a weld over three layers of paint with visible porosity. The contaminated area starts about 21 mm into the weld. A change in the spatter level could be observed during the welding process as soon as the weld pool reached the contaminated area. In addition, a large amount of solidified spatter was found on the plate after the completion of the welds.

Figure 10 shows the measured spatter statistic for welds contaminated with a 0.15-mm layer of paint. The solid red line indicates the 99.9% limit that was calculated using the reference runs. The contaminant begins at about 20 mm for each run, and is indicated with a vertical dotted line. A good correspondence between the crossing of the limit and high values of the spatter statistic can be seen.

When using a pulsed welding process, the influence of paint contamination on the quality of the weld was much less significant. Even with three layers of paint, no visible porosity could be achieved. However, this may be primarily due to the difference in the thickness of the plates. As the pulsed process was not hot enough to achieve good fusion on 9-mm plates, 3-mm plates were used. As the heat capacity of these plates is much lower, it is suspected that they heat up much faster, allowing for the contaminant to vaporize before reaction with the weld pool takes place. Figure 11 shows an example of a weld with contamination from three layers of paint. The paint starts at about 20.5 mm.

Figure 12 shows the spatter statistic for paint contamination for the pulsed process. Generally, the amount of spatter created in pulsed welding is much lower than that created in constant voltage operation. For the pulsed process, the probability of detection is not as high as in the constant voltage case.

Oil

While oil contamination did cause an increase in the overall spatter level, it did not create obvious changes in the solidified weld bead, even with severe contamination. Some beads do show slight cases of necking. However, similar to paint contamination, in the constant voltage runs large amounts of solidified spatter were found in the vicinity of the weld beads, indicating a reaction of the contaminant with the weld pool. Spatter levels increased for all sizes from small to large spatter and were greatest for this type of contamination. Plots of the spatter statistic for the constant voltage process are shown in Fig. 13, and for the pulsed process in Fig. 14. Again, the increase in spatter activity is most evident in the constant voltage weld process.

Conclusions

In this paper, a method of identifying spatter events and tracking spatter objects has been presented. Counting the frequency of spatter events has been shown to be an indicator of the presence of contaminants, i.e., oil and primer paint of excessive thickness. In addition, the number of spatter events of specific size appear to vary as a function of the contaminant type.

The purpose of this research was primarily to prove the concept of contaminant detection based on spatter detection. While this has been achieved, more research is necessary to develop the system into a true contaminant classification system for practical use. In the current configuration, the image processing and spatter tracking are done post-process, but significant optimizations could be applied to be able to process the data online. For example, the algorithms that have been developed to identify and quantify the spatter events could be transferred to field programmable gate arrays (FPGAs). By doing so, the processing time is reduced orders of magnitude, thus making real-time detection possible. The long-term goal of this research is to develop an online weld quality monitor, for automated welding processes, that would identify the presence of containments in real-time, alert supervision, and halt the process, if appropriate, thus reducing or eliminating bad welds and costly rework. While the vision system used in this research was both expensive (~$3000) and too intrusive into the

welding gun/workpiece workspace, the long-term plan is miniaturization of the camera to be less intrusive. This plan is supported by recent hardware developments in cameras and imaging, such as cell phone and car backup cameras. This work helps pave the way for online vision-based monitoring of welding processes in automated workcells — a development that will help productivity and quality.

Acknowledgment

Supported in part by NSF grants 0116753 and 0134132.

References

1. Kang, S. K., and Na, S. J. 2005. A mechanism of spatter production from the viewpoint of the integral of specific current action. *Welding Journal* 84(12): 188-s to 196-s.

2. Kang , M. J., Kim, Y., Ahn, S., and Rhee, S. 2003. Spatter rate estimation in the short-circuit transfer region of GMAW. *Welding Journal* 82(9): 238-s to 247-s.

3. Kang, M. J., and Rhee, S. 2001. The statistical models for estimating the amount of spatter in the short-circuit transfer mode of GMAW. *Welding Journal* 80(1): 1-s to 8-s.

4. Baune, E., Bonnet, C., and Liu, S. 2001. Assessing metal transfer stability and spatter severity in flux cored arc welding. *Science and Technology of Welding and Joining* 6(3): 129–148.

5. Chen, J. H., Sun, Z. C., and Fan, S. D. 1996. Study on the mechanisms of spatter produced by basic welding electrodes. *Welding Journal* 75(10): 311–316.

6. Molleda, F., Mora, J., Molleda, J. R., Mora, E., and Mellor, B. G. 2007. The importance of spatter formed in shielded metal arc welding. *Materials Characterization* 58: 936–940.

7. Yuichi, I., Hidedi, M., Shin'ya, Y., and Masato, U. Effects of shielding gas for spatter reduction of GMAW. *J. Japan Welding* 75(7): 570–574.

8. Kovacecic, R., and Zhang, Y. M. 1997. Real-time image processing for monitoring of free weld pool surface. *Journal of Manufacturing Science and Engineering* 140(3): 161–169.

9. Bae, K.-Y., Lee, T.-H., and Ahn, K.-C. 2002. An optical sensing system for seam tracking and weld pool control in gas metal arc welding of steel pipe. *Journal of Materials Processing Technology* 120: 458–465.

10. Zhao, D. B., Chen, S. B., Wu, L., Dai, M., and Chen, Q. 2001. Intelligent control for the shape of the weld pool in pulsed GTAW with filler metal. *Welding Journal* 80(11): 253-s to 260-s.

11. Mnich, C. 2004. Development of a synchronized, high-speed, stereovision system for in situ weld pool measurement. Master's thesis, Colordo School of Mines, Golden, Colo.

12. Guangjun, Z., Zhihong, Y., and Lin, W. 2006. Reconstructing a three-dimensional P-GMAW weld pool shape from a two-dimensional visual image. *Measurement Science and Technology* 17(7): 1877–1882.

13. Jain, A. K. 1989. *Fundamentals of Digitial Image Processing*, p. 384, Englewood Cliffs, N.J., Prentice Hall.

14. Reid, D. 1979. An algorithm for tracking multiple targets. *IEEE Transactions on Autonatic Control* 24(6): 843–854.

15. Blackman, S. S. 2004. Multiple hypothesis tracking for multiple target tracking. *IEEE Aerospace and Electronic Systems* 19(1): 5–18.

16. Bar-Shalom, Y., and Rong Li, X. 2003. *Estimation with Applications to Tracking and Navigation*, New York, N.Y., Wiley.

17. Schwab, G. 2008. Spatter detection and contaminant classification in robotic gas metal arc welding. PhD thesis, Colorado School of Mines.

18. Yates, R. D., and Goodman, D. J. 2005. *Probability and Stochastic Processes,* New York, N.Y., Wiley.

19. Bouguet, J.-Y. 2007. Camera calibration toolbox for Matlab, online paper. *www.vision.caltech.edubouguetj/calib_doc/*

20. Bell, B. 1994. The iterative Kalman smoother as a Gauss Newton method. *SIAM J. Optimization* 4(3): 626–636.

Preparation of Manuscripts for Submission to the *Welding Journal* Research Supplement

All authors should address themselves to the following questions when writing papers for submission to the Welding Research Supplement:

- Why was the work done?
- What was done?
- What was found?
- What is the significance of your results?
- What are your most important conclusions?

With those questions in mind, most authors can logically organize their material along the following lines, using suitable headings and subheadings to divide the paper.

1) **Abstract.** A concise summary of the major elements of the presentation, not exceeding 200 words, to help the reader decide if the information is for him or her.

2) **Introduction.** A short statement giving relevant background, purpose, and scope to help orient the reader. Do not duplicate the abstract.

3) **Experimental Procedure, Materials, Equipment.**

4) **Results, Discussion.** The facts or data obtained and their evaluation.

5) **Conclusion.** An evaluation and interpretation of your results. Most often, this is what the readers remember.

6) **Acknowledgment, References and Appendix.**

Keep in mind that proper use of terms, abbreviations, and symbols are important considerations in processing a manuscript for publication. For welding terminology, the *Welding Journal* adheres to AWS A3.0:2001, *Standard Welding Terms and Definitions*.

Papers submitted for consideration in the Welding Research Supplement are required to undergo Peer Review before acceptance for publication. Submit an original and one copy (double-spaced, with 1-in. margins on 8 ½ x 11-in. or A4 paper) of the manuscript. A manuscript submission form should accompany the manuscript.

Tables and figures should be separate from the manuscript copy and only high-quality figures will be published. Figures should be original line art or glossy photos. Special instructions are required if figures are submitted by electronic means. To receive complete instructions and the manuscript submission form, please contact the Peer Review Coordinator, Erin Adams, at (305) 443-9353, ext. 275; FAX 305-443-7404; or write to the American Welding Society, 550 NW LeJeune Rd., Miami, FL 33126.